This is a repository copy of *Magnetohydrodynamic instabilities of double magnetic bands in a shallow-water tachocline model. II. teleconnection between high- and low-latitude bands and across equator*.

White Rose Research Online URL for this paper:
https://eprints.whiterose.ac.uk/220618/

Version: Published Version

CrossMark

Magnetohydrodynamic Instabilities of Double Magnetic Bands in a Shallow-water Tachocline Model. II. Teleconnection Between High- and Low-latitude Bands and Across Equator

Mausumi Dikpati[1] , Bernadett Belucz[2,3] , Robertus Erdélyi[2,3,4] , Peter A. Gilman[1] , Scott W. McIntosh[1,5] , and Breno Raphaldini[1]

[1] High Altitude Observatory, NSF-NCAR, 3080 Center Green Drive, Boulder, CO 80301, USA; dikpati@ucar.edu
[2] Solar Physics and Space Plasma Research Center, School of Mathematics and Statistics, University of Sheffield, S3 7RH, UK
[3] Hungarian Solar Physics Foundation, Gyula, Hungary
[4] Department of Astronomy, Institute of Geography and Earth Sciences, Eötvös University, Budapest, Hungary
[5] Lynker Space, Boulder, CO 80301, USA

Abstract

The "extended solar cycle" indicates that there are two deeply seated toroidal magnetic field bands in each hemisphere. Both bands migrate equatorward as a sunspot cycle progresses. Here, we examine the consequences of global MHD instability of this migrating double-band system in tachocline on the latitudinal structure of unstable modes, which are essentially MHD Rossby waves. We find that latitude-location, latitude-separation, and the amplitude of the bands strongly influence the latitudinal structure and growth rates of the unstable modes of both symmetries about the equator. These properties can lead to "teleconnections" between low- and high-latitudes in each hemisphere and across the equator. High-latitude bands can destabilize low-latitude bands that would otherwise be stable. Stronger high-latitude bands lead to strong interactions between low and high latitude in each hemisphere, but inhibit cross-equatorial band-interaction. Strong cross-equatorial interactions of modes can synchronize cycle minima in north and south. Symmetric and antisymmetric modes of similar amplitudes can lead to substantial asymmetries between north and south. As a solar cycle progresses, excited MHD Rossby waves go through a sequence of changes in latitude structure and growth rate, while maintaining strong links in latitude. These changes and links are theoretical evidence of teleconnections between widely separated latitudes and longitudes in the Sun, which may explain many of the evolving surface magnetic patterns observed as a solar cycle progresses. The wider the separation between high- and low-latitude bands, the earlier the cross-equatorial teleconnection starts in a cycle, and hence the earlier the cycle starts declining.

Unified Astronomy Thesaurus concepts: Solar activity (1475); Magnetohydrodynamics (1964); Solar interior (1500); Solar photosphere (1518); Solar cycle (1487)

1. Introduction

Solar observation and modeling studies provide evidence of the existence of extended solar cycles (ESCs). The first extensive review of observations of ESCs can be found in E. W. Cliver (2014). To mention a few specific examples of the evidence of ESCs, we include, for instance, patterns of the torsional oscillation (R. Howard & B. J. Labonte 1980; H. B. Snodgrass & P. R. Wilson 1987; G. A. Guerrero et al. 2016), ephemeral active regions (K. L. Harvey & S. F. Martin 1973; S. F. Martin 2018), prominences and filaments (G. Bocchino 1933; R. Hansen & S. Hansen 1975), the coronal green line emission (S. J. Tappin & R. C. Altrock 2013), and global-scale features of the Sun's corona (R. C. Altrock 1988). These observations may indicate that the solar activity cycles start at higher latitudes (around 60°–70°) at a weak level ahead of the start of the actual sunspot cycle. This high-latitude branch already appears around 60° latitude when the low-latitude branch is at ∼30° latitude. While the former does not produce sunspots but rather only weak ephemeral regions, the latter is responsible for solar activity

cycle. These two branches are observed to gradually move toward the equator with the progress of the solar cycle. Eventually, the low-latitude branch or active-cycle branch reaches the equator and annihilates with its opposite-hemisphere counterparts. The resulting situation could cause a solar "tsunami" that activates the high-latitude branch, which reaches about 30° by that time, and triggers the birth of the new cycle's spots (M. Dikpati et al. 2019). The annihilation could create a void, into which the plasma flows from the poleward side of the magnetic band. That plasma was essentially supporting the magnetic band from a poleward slip. Then, the excess plasma overflows back toward the pole in the form of poleward propagating gravity waves, which perturb the high-latitude band to stimulate spot emergence. P. R. Wilson (1987) described this spatio-temporal extension of solar activity to higher solar latitudes as the ESC. J. L. Leroy & J. C. Noens (1983) found extended cycle of coronal activity patterns with about 17 yr periods from the analysis of coronal emission and morphology from Pic-du-Midi observatory, consistent with the previous findings by J. P. Legrand & P. A. Simon (1981) from 100 year geomagnetic index analysis.

A plausible origin of such a double-branch migration equatorward in a coherent fashion could be a pair of double bands, one pair in each hemisphere, deeper down from the surface, generated by a dynamo (M. Dikpati & P. Charbonneau 1999) at/near the base of the convection zone or tachocline, with oppositely

signed bands at high and low latitudes in each hemisphere. A recent study has discussed the concept of a dynamo driven by magnetorotational instability in the near-surface shear layer (G. M. Vasil et al. 2024), but their model does not address why the same magnetorotational instability would not occur also in the tachocline. Such a magnetorotational instability has indeed been found to occur in the tachocline by many authors (D. Kagan & J. C. Wheeler 2014; P. A. Gilman 2018; G. Mamatsashvili et al. 2019). Thus, if the magnetorotational instability can play a role in solar dynamo occurring at the surface, such a dynamo can also occur in the tachocline, where the large-scale coherent magnetic structures are more likely to be sustained. There have been attempts to simulate ESCs, with partial success. Nonetheless, the ESCs are evident from various observations. A comprehensive recent review by A. K. Srivastava et al. (2018) describes various observations supporting the existence of ESCs. A plausible origin of ESCs may be the tachocline, where the dynamo generates the strong toroidal fields from which active regions emerge at the surface through some recipes of flux emergence. In this scenario, the global MHD tacholine instabilities can create bulges and depressions in the plasma fluid; magnetic fields coinciding with the bulges are more likely to be pushed up through the convection zone to make their buoyant rise to the surface. The latitude–longitude locations of these bulges are the "imprints" for flux-emergence locations (see, e.g., Figure 11 of M. Dikpati & S. W. McIntosh 2020). However, note that all flux-emergence recipes rely on a threshold field strength (about 15 kG), above which the flux would emerge from the tachocline to the surface, taking a rise-time of about a few months (M. A. Weber et al. 2013).

Given their existence, what can an ESC tell us about the properties of the sunspot cycle itself? B. Belucz et al. (2023) studied the global MHD of a double-banded toroidal system in the tachocline to explore its implications for the properties of solar activity and the solar cycle. They found that the high- and low-latitude bands interact in the same hemisphere when their latitude-separation is 30°, such as when they are at latitude 60° and 30°, respectively. The double-band system does not interact with the opposite-hemisphere counterpart across the equator until the low-latitude bands in the north and south are separated by less than 30°. This means that their cross-equatorial interaction starts after the high- and low-latitude bands in each hemisphere arrive at latitudes of 45° and 15°, respectively. This happens to be when the solar cycle reaches its peak. An optimal separation between the low-latitude bands in two hemispheres is 30° for starting the interaction across the equator. As the cycle passes through the peak and starts declining, this latitudinal separation decreases, allowing more interaction across the equator.

The physics of the band-interaction across the equator has been described by B. Belucz et al. (2023; see also A. Strugarek et al. 2023) as an example of a "teleconnection." In climate studies, teleconnection is a general concept used to explain various long distance, dynamic correlations that are caused by a signal of a physical process occurring in one geographical location that is communicated or transmitted to a widely separated location. There it induces a physical response (E. N. Lorenz 1951; B. J. Hoskins & D. J. Karoly 1981; K. E. Trenberth et al. 1998; A. S. W. Teruya et al. 2024) that helps explain, for example, geographically widely separated, time dependent, climatic anomalies, such as the well-known El Nino Southern Oscillation. In the earth's atmosphere,

teleconnections come from energetically active Rossby wave patterns (i.e., the ones having tilts), as well as packets of Rossby waves carrying kinetic energy over great geographical distances before "breaking" and depositing that energy to change the weather in the location where the waves broke (B. J. Hoskins & T. Ambrizzi 1993; N. Boers et al. 2019). In the Sun, tilted patterns of Rossby waves are generated by the global MHD tachocline instability. Essentially, the Rossby waves form from the perturbations to the unperturbed reference states of magnetic fields and differential rotations and can grow (decay) by extracting energy from (depositing energy to) the unperturbed differential rotation and magnetic field via the action of Reynolds, Maxwell, and mixed stresses (M. Dikpati et al. 2018a). As a result of this interaction among Rossby waves and unperturbed reference states, axisymmetric toroidal magnetic bands in each hemisphere bend or tip to form non-axisymmetric patterns in such a way as to come closer to each other at certain longitudes locally, and tip-away at certain other longitudes (see Figure 4 in P. S. Cally et al. 2003).

This type of mechanism of communication between remote regions via Rossby wave dynamics, though well-established in the Earth's atmospheric phenomena (J. M. Wallace & D. S. Gutzler 1981; N. Boers et al. 2019), was relatively recently discovered to exist in the Sun (R. J. Leamon et al. 2021), suggesting that Rossby waves in the Sun's interior could also play a role (A. S. W. Teruya et al. 2022). Clearly, there are significant differences between conditions affecting the Earth's global atmosphere and the Sun. The Earth has fixed continents and oceans as boundary conditions on the atmosphere, which have no counterparts in the Sun, while the Sun has strong dynamically significant magnetic fields that themselves display global organization, manifested in the properties of sunspot cycles and the solar corona. Magnetic fields play no role in the Earth's lower atmosphere global dynamics. Despite these differences, the Sun and Earth have ubiquitous, global-scale Rossby waves in common. Therefore, the two systems can both be experiencing forms of teleconnection.

B. Belucz et al. (2023) showed that the optimal separation between oppositely directed toroidal bands is about 30° for triggering the teleconnection mechanism. Therefore, at the beginning of a solar cycle, when the high-latitude band is at ∼60° and the low-latitude band is at ∼30° in each hemisphere, the high- and low-latitude bands fulfill the criteria of the band separation in latitude in each hemisphere and can interact via teleconnection. However, the two low-latitude bands in the northern and southern hemispheres are separated by much more than 30°, and hence cannot interact across the equator. Their interaction starts when they reach 15° latitude in each hemisphere. This is the peak phase when the interaction starts. As they drift further toward the equator, the cross-equatorial interaction increases while the cycle declines.

While the observations indicate a roughly 30° separation between the high- and low-latitude bands in each hemisphere, Figure 1 reveals that this separation could vary from 20° to 40°. This leads us to ask the following: (i) Do the high- and low-latitude bands in each hemisphere interact more effectively when they are 20° separated and less so when their separation is 40°? (ii) Do the interactions between low-latitude bands in the northern and southern hemispheres also change accordingly? (iii) Does this impact the timing of the peak of the solar cycle?
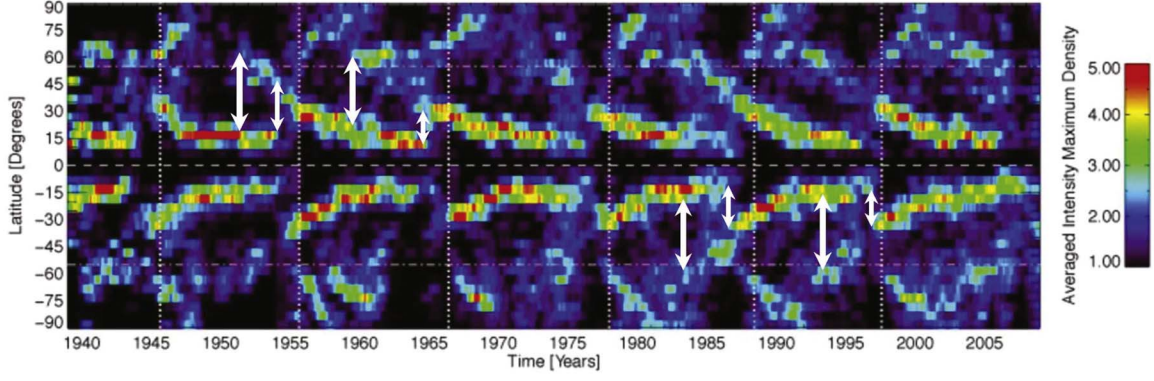
Figure 1. ESC reveals that the separation between high- and low-latitude branches in each hemisphere may not be constant but may vary with the progress of the cycle. Adapting Figure 7(d) from S. W. McIntosh et al. (2021; the extended cycle in NGDC green line), the double-arrows are overlaid on the extended cycle. This reveals that the high- and low-latitude branches are more than 30° separated at the beginning of a solar cycle but their separation decreases as the cycle progresses.

The organization of our paper is as follows. Section 2 describes the MHD shallow-water model, which is the same as that used in B. Belucz et al. (2023), where the governing equations are given in detail; hence, we will skip showing the equations here. Section 3 presents the results, including the physical properties of the instability that are responsible for producing a teleconnection in latitude, as well as how the instability intensity is related to Alfvén waves and latitude-separation between high- and low-latitude bands. Section 4 presents a summary and conclusions.

2. Model

In our previous article, (B. Belucz et al. 2023) we described the MHD shallow-water model in detail; here, we present just a short description. The model is for a thin conducting fluid shell with a rigid bottom and deformable top surface. In this model, the horizontal velocities and magnetic fields are much larger than their vertical counterparts. An MHD shallow-water model has been employed by many authors in the solar context (P. A. Gilman 2000; T. V. Zaqarashvili et al. 2007; D. A. Klimachkov & A. S. Petrosyan 2017), as well as in the context of highly magnetized astrophysical bodies, such as the Keplarian disk (O. Umurhan 2008). Details of the formalism and the equations for a thin spherical shell rotating with the core-rotation rate of the Sun can be found in earlier papers, such as M. Dikpati et al. (2018a) or B. Belucz et al. (2023).

The velocity and the magnetic field are defined as $V = u\hat{\lambda} + v\hat{\phi}$ and $\boldsymbol{B} = a\hat{\lambda} + b\hat{\phi}$, where $\hat{\lambda}$ and $\hat{\phi}$ are unit vectors in the longitudinal and latitudinal directions. The radial velocity (w) is a linear function of height. The nondimensional unit of length and time are the radius (r_0) and inverse of the interior rotation rate (ω_c).

The nondimensional effective gravity, G, is defined as $G \sim 10^3 |\nabla - \nabla_{ad}|$, for the overshoot layer of tachocline is $10^{-2} \lesssim G \lesssim 10^{-1}$, and in the radiative tachocline is $10^1 \lesssim G \lesssim 10^2$.

The latitudinal differential rotation, as derived from helioseismology, can be expressed in the rotating frame as

$$\omega_0 = s_0 - s_2 \mu^2 - s_4 \mu^4 - \omega_c, \qquad (1)$$

where μ is the sine latitude and s_0, s_2, and s_4 are coefficients. The interior rotation rate (ω_c) approximately matches the rotation rate at 32° latitude at the tachocline. The s_0 parameter

is the rotation rate at the equator and the differential rotation amplitude becomes $(s_2 + s_4)/s_0$ (M. Dikpati et al. 2018a).

We prescribed the latitudinal profile of the band as

$$\alpha_0 = p_h f_{0h} (e^{-\beta_h (\mu - d_{sh})^2} - e^{-\beta_h (\mu + d_{sh})^2})$$
$$+ p_l f_{0l} (e^{-\beta_l (\mu - d_{sl})^2} - e^{-\beta_l (\mu + d_{sl})^2}). \qquad (2)$$

In expression (2), f_{0n} is the field strength ($f_{0n} = 0.1$ is 10 kG in real units), β_n controls the width of the toroidal field band, d_{sn} is the sine latitude of the center of the band, and p_n are the prefactors to scale the peak-field strength with the change in β_n in the Gaussian profile, so that the value of f_{0n} denotes the peak-field strength ($n = h$, l shows the parameters of high-latitude and low-latitude bands).

3. Results

Before examining growth rate contours for instability, as well as unstable eigenfunctions in detail, it is important to point out relevant general features of the joint instability of latitudinal differential rotation and banded toroidal field profiles. Unstable perturbations grow in the form of longitudinally propagating waves. These unstable waves have some properties of magnetically modified Rossby waves in the MHD case, and Rossby waves modified and constrained by the differential rotation in the HD case. As such, these waves are distinct from classical Rossby waves found in uniformly rotating thin spherical shells (B. Haurwitz 1940), as well as from "pure" Alfvén waves such as are found in conducting fluids with uniform fields. Unstable waves extracting kinetic and/or magnetic energy from differential rotation and toroidal fields must have longitudinal phase velocities that fall within the range of latitudinal differential rotation in the system (P. A. Gilman & P. A. Fox 1997; M. Dikpati & P. A. Gilman 1999), regardless of the strength of the toroidal field. Waves that are moving either faster or slower have less ability to be modified by the differential rotation in situ to form the perturbation structure needed to extract energy. Therefore, they stay neutral energetically, and if excited would have to have received their energy from a source other than instability of differential rotation or toroidal fields.

We know from previous work that for a single band, the latitude of its placement influences disturbance growth rates because at different latitudes the same band experiences differing amounts of differential rotation across the band. We also know that unstable mode velocities extend well away from

the band, while magnetic perturbations must remain close to the band latitude, indicating that the interactions between bands, whether in a single hemisphere or across the equator, are carried out by the velocities, along with the pressure field, but probably less so by the magnetic perturbations themselves. But we also expect unstable modes with opposite symmetry about the equator to be excited; one symmetry allows latitudinal flow perturbations to cross the equator, while the other contains latitudinal magnetic perturbations that cross the equator. So, both magnetic fields and velocities can link the two hemispheres. In addition, with two bands present, it is possible for one band, particularly the low latitude one, to act as a barrier to the velocity perturbations reaching beyond that band, which limits interaction with the opposite hemisphere. All these features, which are absent in the HD case, can help us interpret the instability growth rates and unstable disturbance patterns we find.

Kinetic energy of unstable modes is extracted from differential rotation by growing perturbations that acquire a "tilted" structure in latitude of the perturbation streamlines, with those at lower local rotation lagging those at higher local rotation. The tilt implies a correlation between longitude and latitude components of velocities in the disturbance, implying a Reynolds stress that transports angular momentum down the rotation gradient, from lower latitudes to higher ones. The amplitude of the perturbations is maximum at or near the latitude where the latitude gradient of the total vorticity (i.e., the sum of the coordinate system vorticity and the relative vorticity of the differential rotation itself) changes sign; the phase speed of the unstable wave is close to the local rotation speed at the latitude of the inflection point. The vorticity sign change is a necessary condition for instability in the 2D case. In the shallow-water case, it is modified to be the location where the total "potential vorticity" gradient changes sign, potential vorticity being defined as the total vorticity divided by the local thickness of the shallow-water layer (M. Dikpati & P. A. Gilman 2001). For the solar differential rotation profiles of the form $s_0 - s_2 \sin^2 \phi - s_4 \sin^4 \phi$, where ϕ is latitude, the s_4 term guarantees that there is a sign change in the latitude rotation gradient at a relatively high latitude, typically around 60°, implying instability whose disturbances peak at high latitudes.

When a toroidal band system is added, the instability gets enhanced, due to availability of additional energy source, namely the magnetic energy. Maxwell stresses arising from tilted total magnetic field lines (unperturbed reference state plus perturbation magnetic fields) can extract kinetic energy from the differential rotation, whereas a "mixed" stress, arising from cross-correlation of the perturbation latitudinal flow with longitudinal magnetic field and longitudinal flow with latitudinal field, can extract magnetic energy out of the toroidal band. Structurally, this energy extraction arises from a phase shift in longitude between the perturbation velocities and their magnetic counterparts, which can clearly be seen in the eigenfunction plots later on. However, the hydrodynamic instability generally can still coexist.

The single-band case has been studied extensively (M. Dikpati & P. A. Gilman 1999; M. Dikpati et al. 2003) for a wide range of band strengths, widths, and placement in latitude. But the double band case has only been studied so far by B. Belucz et al. (2023) for a restricted set of band placements. If two oppositely directed bands are close to each other, there exists the possibility of cancellation of perturbation flux, and therefore magnetic energy. This can occur within a single hemisphere, or across the equator. Which of the two energy extraction mechanisms is more important depends primarily on the magnetic field amplitude of the band. The stronger the peak field is, the more energy comes from the magnetic field compared to that coming from the differential rotation. But in all cases some differential rotation must be present for the instability to happen. The larger the rotation gradient across the band, the stronger is the instability. A perturbation whose phase speed in longitude is substantially different from the local rotation at the latitude of the toroidal field peak will not be able to establish the steep longitude phase shifts with latitude in the velocity and magnetic perturbations across the width of the band. With two bands present, it is impossible to optimize the energy extraction from both bands with a single unstable eigenfunction because it has to have a single longitude phase speed. But there can be two unstable modes for the same longitude wavenumber, each one with a phase velocity optimized to extract magnetic energy from one of the toroidal bands. We will see that in the solutions we display.

### 3.1. Unstable Disturbance Growth Rates

We performed a detailed survey of growth rates of $m = 1$ unstable modes for both symmetries for 40° (Figure 2) and 20° (Figure 3) separation. For all cases, we set $G = 0.5$, a plausible value for a one layer tachocline.

In general, in the case of a double-band system there can be more than one unstable mode for the same parameter values because each band can act as a distinct energy source for instability. In Figures 2 and 3, we have shown growth rates only for the most unstable mode because it is likely that the mode that will dominate if the disturbance is allowed to grow to finite amplitude. For different parameter values, which mode is the most unstable for the same m can change, resulting in different growth rate "regimes" in a map of growth rate contours.

We show the contours of growth rates for band pairs placed at declining latitudes from top to bottom in Figures 2 and 3. In each panel, the vertical axis is the peak-field strength of the low-latitude band; the horizontal axis is the same for the higher latitude band. The four frames in the left-hand column show the antisymmetric modes and the right-hand column shows the symmetric modes. The lighter color shading denotes higher growth rates and the darkest color the slowest growth rates. In B. Belucz et al. (2023), we found growth rates of disturbances for double bands with 30° separation in their latitude locations.

It is useful to discuss Figures 2 and 3 together; they have some properties in common but also differences. For example, for both band separations, as the low-latitude band gets close to the equator, the growth rates are smaller (shading gets darker). This is more pronounced in the 20° separation case because the high-latitude band is much closer to the equator. This effect probably comes from the fact that latitude differential rotation is weaker at the lowest latitudes, making less kinetic energy available for instability of the combined bands and differential rotation.

For both band separations and both symmetries, when the band pair is placed closer to the equator, instability of the low-latitude band disappears completely, and the high-latitude band peak is weaker. This effect is clearly stronger for the narrower band separations, with symmetric mode instability absent regardless of high-latitude band amplitude for lower amplitude
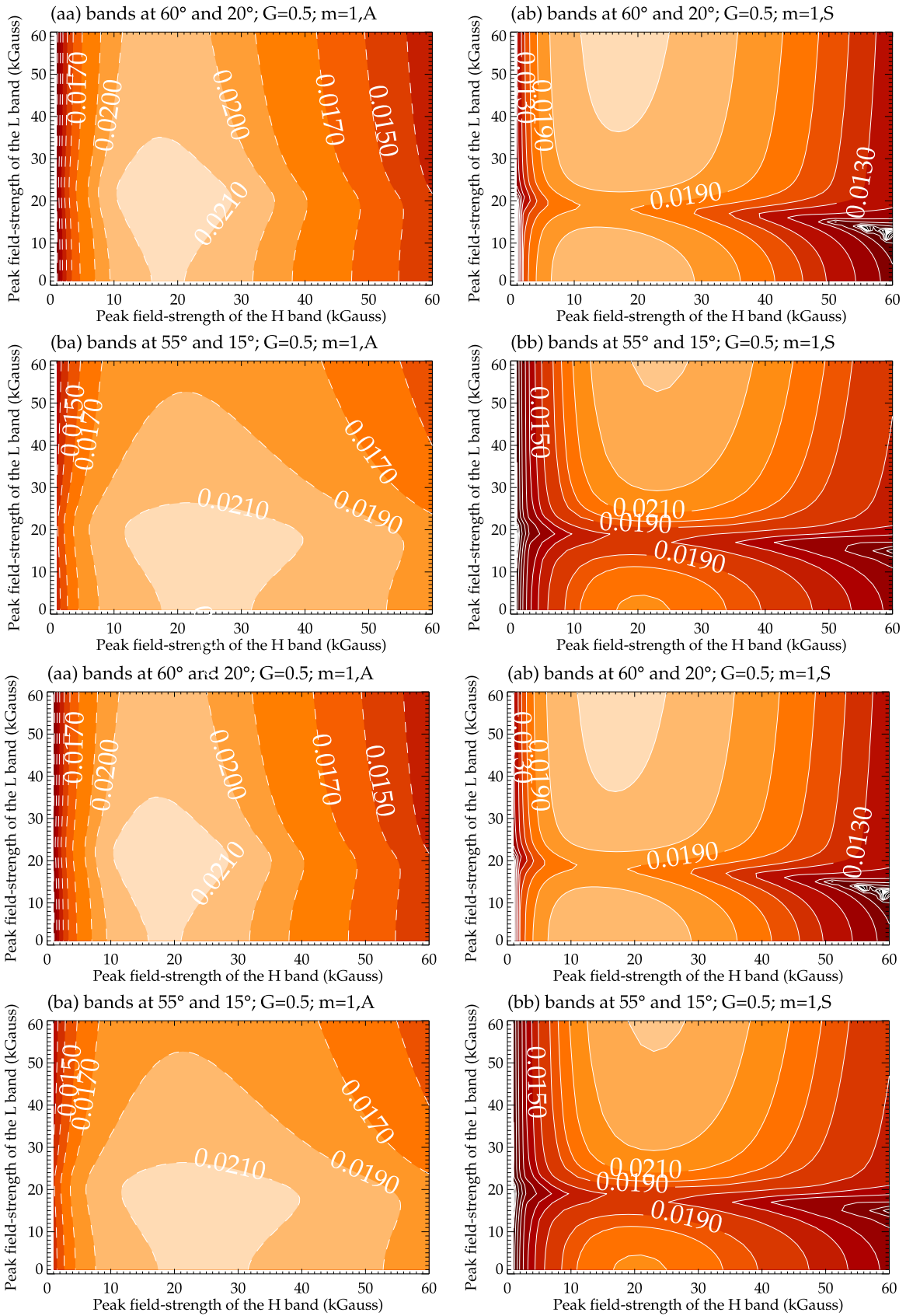
Figure 2. For $G = 0.5$, growth rate contours for $m = 1$ modes are displayed in the field-strength space, in which the x-axis denotes the strength of the high-latitude band, denoted by H band in the x-axis label, and the y-axis that of the low-latitude band, denoted by L band in that label. Left-hand and right-hand panels are, respectively, for antisymmetric ($m = 1, A$) and symmetric ($m = 1, S$) modes. As the band system migrates from high latitudes toward the equator, the four rows from top to the bottom show how the instability features change, respectively, for bands at 60°–20° (aa, ab), 55°–15° (ba, bb), 50°–10° (ca, cb), and 45°–5° (da, db).
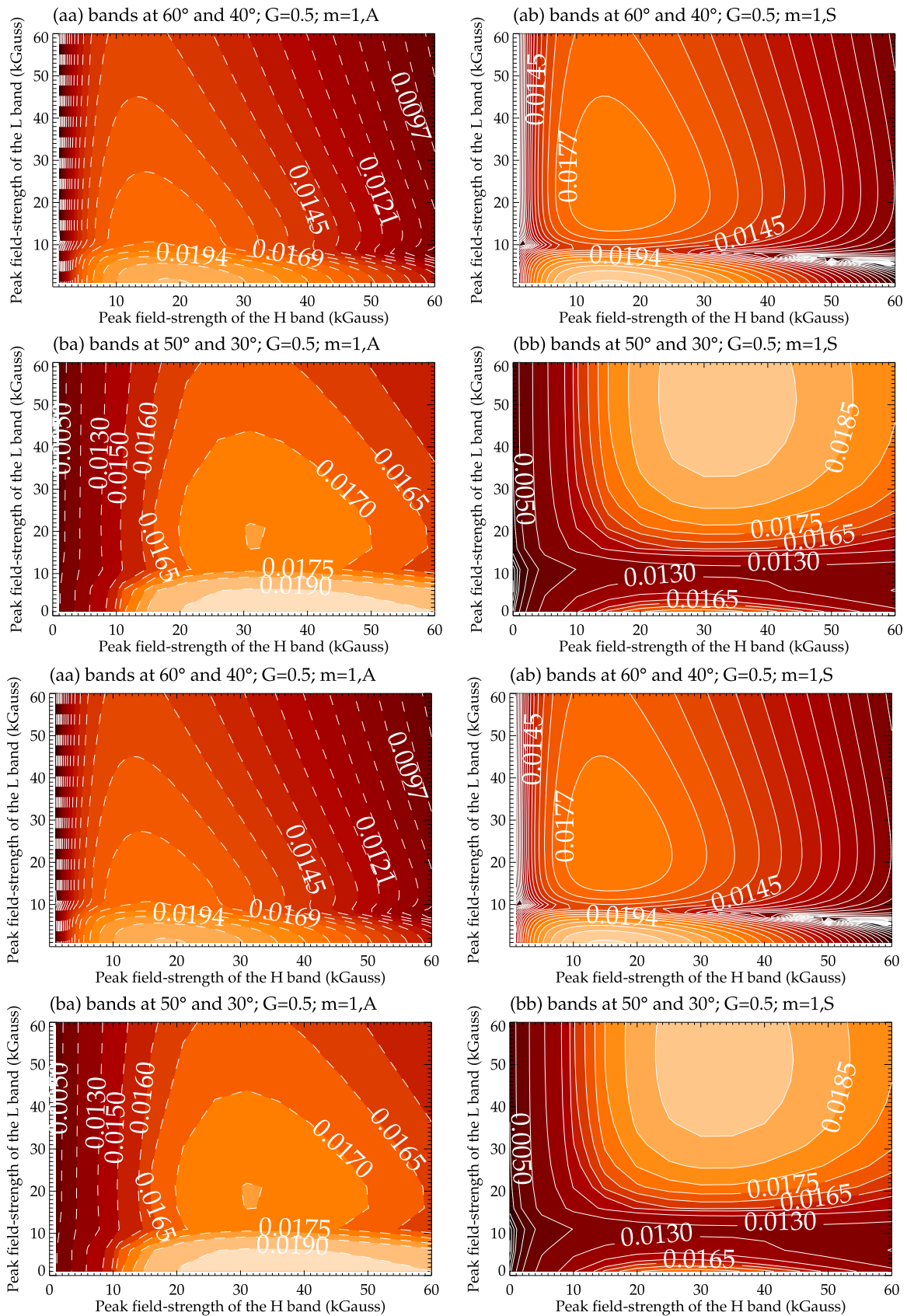
Figure 3. The same as in Figure 2, but for 20° band separation.

lower latitude bands. Antisymmetric modes require a high-latitude band with peak strength between 10 and 20 kG, depending on the low-latitude band peak. Even when there is instability, the growth rates are rather small, implying e-folding growth times of a few years. So, there are limits to the high-latitude band's causing instability of the low-latitude band.

For bands separated by 20°, for symmetric modes, instability disappears altogether when the low-latitude band reaches 5°, while antisymmetric modes are stable for high-latitude bands of 15 kG strength or less, no matter what the low-latitude band strength.

A second feature in common is that as the band pair moves closer to the equator, the peak in disturbance growth rates migrates to a higher peak in the high-latitude band. In other words, it takes a stronger high-latitude band and therefore more magnetic energy available to make the whole system unstable. A third common feature is that for both band separations there are different growth rate domains for weak and strong peaks in the low-latitude band. This feature is more pronounced for equatorially symmetric than antisymmetric modes. This is an example of different unstable eigenfunctions for the same wavenumber m. Each is extracting energies from different energy sources to grow. We return to this point in the discussion of later figures. For bands separated by 20°, the boundary between the two growth rate regimes occurs for low-latitude bands of about 10 kG. For band separation of 40°, the regime change, again most clearly seen for symmetric modes, occurs for low-latitude band peaks near 20 kG.

For both the 20° and 40° band separations, there is an additional effect at work, which is different for the two different separations. For single bands, the amount of instability depends in part on where the band is located with respect to the local the differential rotation because the instability is realized by the local rotational shear across the band. The latitude where the maximum shear occurs is a function of the total profile of differential rotation from the equator to pole, which generally peaks at or near 45°. So, the high-latitude band instability will be strongest near that latitude. This effect is particularly important for the case of 40° separation. With 20° separation, when the low-latitude band is at 5°, the high-latitude band is at 25°, implying that the band will be less unstable.

Regardless of the fact that in these calculations, while there are always two toroidal bands in each hemisphere, the unstable eigenfunctions are truly global, with different latitude structures for opposite symmetries, we can ask this question: As a function of the parameters of the problem, which toroidal band has the greatest contribution to the instability? The way to answer this question from the results in Figures 2 and 3 is to realize that where the growth rate contours are nearly vertical, signifying growth rate nearly independent of the low-latitude band's peak amplitude, the instability is determined by the strength of the high-latitude band. This will also be evident in the structure of the eigenfunctions shown in later figures. Conversely, when the growth rate contours are nearly horizontal, the strength of the low-latitude band dominates in the instability.

If we apply these inferences to Figure 2, we see that for weak high-latitude bands (near left boundary of all frames), the growth rate is nearly independent of the low-latitude band peak. This is clear evidence of a strong linkage between low and high latitudes for even weak high-latitude bands. This

effect is most pronounced for antisymmetric modes, but is present for symmetric modes too. We infer that this implies that the appearance of a new toroidal band at high latitudes can enhance magnetic activity in the declining phases of the present cycle, at least until the low-latitude band is unstable, i.e., until the band is not too close to the equator. We regard this result as evidence of a teleconnection between high and low latitudes, first suggested by S. W. McIntosh et al. (2021). It may influence the late stages of the present cycle, as well as the timing of the appearance of the next one.

We can also see from Figures 2 and 3 that for low-latitude bands, a wide range of field strengths are actually destabilized by the presence of a new high-latitude band of intermediate strength. Even if the low-latitude band is unstable without a high-latitude band present, its growth rate is much larger when the high-latitude band is present, indicating the release of magnetic energy by the unstable high-latitude band through the perturbations (mainly velocities, since they have much wider extent in latitude) to destabilize the low-latitude band. This can lead to a stronger current sunspot cycle. Taking this reasoning a step further, namely why the instability could help spot emergence, we can refer to Figure 11 of M. Dikpati & S. W. McIntosh (2020), which displays that the toroidal magnetic band coinciding with bulges in tachocline fluid (i.e., region of high pressure-departure relative to the surrounding) is more prone to emerge through the convection zone. Thus, it is possible that the instability due to the appearance of a new high-latitude toroidal band can cause a later phase rise in activity from the low-latitude band, perhaps leading to a double maximum in sunspot number for that cycle. That second peak in activity with time might also extend that sunspot cycle in that hemisphere.

For much higher amplitude peaks of the low-latitude band, the growth rate contours are much more horizontal, indicating that the low-latitude band is determining the strength of the instability. By inference, for such high fields, the influence of a weak high-latitude band is much less. However, such high fields close to the equator may be unrealistic for the Sun. Magnetic buoyancy instability for toroidal fields significantly above 10 kG in peak value should have already erupted as sunspots (P. A. Gilman 2018).

When we look for the same effects in Figure 3, for which the band separation is just 20°, we see vertical growth rate contours extending to even higher peaks in the low-latitude band. We also see it for both mode symmetries. So, in this case the closeness in latitude of the high-latitude band to the low-latitude one makes its influence even stronger. A growth rate contour map for intermediate separations, such as 30°, studied in B. Belucz et al. (2023), show similar features to those shown here. Therefore, the influence of a weak, high-latitude toroidal band, representing the start of a new sunspot cycle, is a robust feature of the double banded system, and needs to be taken into account in both observational analyses and model simulations of sunspot cycles.

The horizontal and vertical axes in each plot represent limits for which one of the bands is absent; the horizontal axis has no low-latitude band; the vertical axis has no high-latitude band. From Figure 2 we can clearly see instability of antisymmetric modes extends all the way down to zero amplitude low-latitude bands. As the low-latitude band peak rises vertically on the plot, the low-latitude band starts to interfere with the instability of the high-latitude band, lowering the growth rate, but as the

low-latitude band gets stronger still, it can supply more energy for instability, with the high-latitude band triggering instability of the low-latitude band. The unstable disturbance eigenfunctions should look significantly different in the two regimes. The regime change in growth rate occurs at a higher low-latitude band strength when the band separation is larger because the perturbations associated with each band, being further separated, are less able to interact to influence instability in the other band.

By contrast, the limit for which the high-latitude band goes to zero, seen close to the left-hand vertical axis on each frame, behaves quite differently. As the vertical axis is approached from the right, decreasing the high-latitude band peak, the growth rates go down monotonically to zero for lower latitudes of band placements and near zero for higher latitude band pairs. This is true for both symmetries and both separations. The two band system becomes stable even before the high-latitude band vanishes, particularly for lowest latitude placement of the band pair. These features come from the fact that if the low-latitude band is low enough in latitude, its single-band instability is very weak because the latitude gradient of differential rotation is weak at low latitudes. Instability of the remaining low-latitude band is weak or zero, even for very high band peaks. Considering the succession of sunspot cycles, we can infer from this result that without a growing high-latitude band for the next cycle, sunspot appearances of the cycle from the low-latitude band may disappear sooner than they would otherwise, leaving even a gap between cycles, signifying a longer than average solar minimum.

In summary, we can explain the results above physically by invoking the three instability mechanisms described at the beginning of this section. For low-latitude bands, the two mechanisms for producing instability are too weak. There is not enough differential rotation to produce the disturbance streamline and magnetic perturbation tilts to produce a Reynolds or Maxwell stress to extract kinetic energy from the weak differential rotation gradient. There is also not enough differential rotation to stimulate the longitude phase shift between the magnetic and velocity perturbations, so no magnetic energy is extracted from the toroidal band by the action of mixed stress.

3.2. Unstable Eigenfunctions and their Teleconnections

The growth rates shown in Figures 2 and 3 reveal how one band can destabilize the other, particularly the lower latitude band, which might be stable if the high-latitude band is not present. One can think of this as a form of teleconnection because the bands are separated by between 20° and 40° in latitude and the magnetic linkage between them is weak because magnetic perturbations are confined to the neighborhood of the latitude of the toroidal band. However, perturbation velocities associated with the unstable high-latitude band easily reach the low-latitude band, perturbing it even when, by itself, that band would be stable. This triggering mechanism happening in the Sun could help to determine the timing of the onset of a sunspot cycle. Figures 4 and 5 give typical examples of the actual eigenfunctions for both symmetries about the equator, for toroidal separations of 40° (Figure 4) and 20° (Figure 5).

In Figure 4, we can see that when the bands are at 55° and 15°, respectively, there are substantial perturbation velocities, and magnetic fields between the bands, associated with top-surface deformations, but very little is happening in the domain straddling the equator between the two low-latitude bands. As the band pair gets closer to the equator, there starts to be more perturbation between the two low-latitude bands, particularly for the antisymmetric modes, but the primary perturbation patterns remain between the bands in one hemisphere, as well as poleward of the high-latitude band. In effect, perturbation velocities associated with the unstable high-latitude band are disturbing the low-latitude band in such a way that it becomes unstable too. We can also see that in between the bands the velocity vectors have a pronounced tilt away from latitude circles. This is evidence of angular momentum getting transported from lower latitudes to higher ones, releasing kinetic energy to drive instability of both toroidal bands, but mainly the one at higher latitudes. When the band pair migrates by just 10° in latitude, the tilt disappears; so the continued instability of the double-band system has to be driven primarily by magnetic energy. Most of the energy for instability is coming from the high-latitude band, due to having a larger rotation gradient across the band.

The teleconnection mechanism here arises in the form of perturbation velocities associated with the unstable high-latitude band reaching the low-latitude band and destabilizing it, or in some cases making it more unstable than it would be without the high-latitude band present. Magnetic fields are not directly involved in this communication by velocities because magnetic field perturbations are confined to the immediate neighborhood of the high-latitude band. This teleconnection has a "reach" of several tens of degrees in latitude, enough to connect toroidal fields of the next cycle to the present one. The main mechanism is the formation of latitudinal tilts in the velocity and magnetic disturbance patterns, which are caused by the longitudinally propagating Rossby waves generated by this instability. Alfvén waves, which also propagate in longitude, would rather be confined to the toroidal bands themselves, and hence are not part of this mechanism. However, Alfvén waves associated with toroidal bands could lead to teleconnections in longitude, which is beyond the scope of the present study.

In the context of an advancing sunspot cycle, we can infer that without the presence of the high-latitude band, the low-latitude band at 5° would not be unstable at all, showing that the presence of a new high-latitude band can actually extend the spot production during the current sunspot cycle. This is because the instability can create the conditions for magnetic flux emergence in the form of sunspots (see, e.g., Figure 11 of M. Dikpati & S. W. McIntosh 2020). If the new high-latitude band happened to develop late, the current spot cycle might end early. We can also see that as the band pair moves closer to the equator, instability of the low-latitude band becomes stronger than it was when it was at a higher latitude, as evidenced by the relative length of perturbation magnetic arrows particularly.

Our interpretation of these results and their connection to sunspot cycles is that instability of a toroidal band coupled with local latitudinal differential rotation contributes to the timing of the appearance of sunspots and their frequency of eruption in both the ascending and descending phases of a cycle. This connection has been discussed in previous papers (M. Dikpati et al. 2018b). By the time that the low-latitude band reaches 5°, the perturbation velocities and magnetic fields are close enough together that they are virtually certain to interact across the equator. Unstable modes of each symmetry have one latitudinal
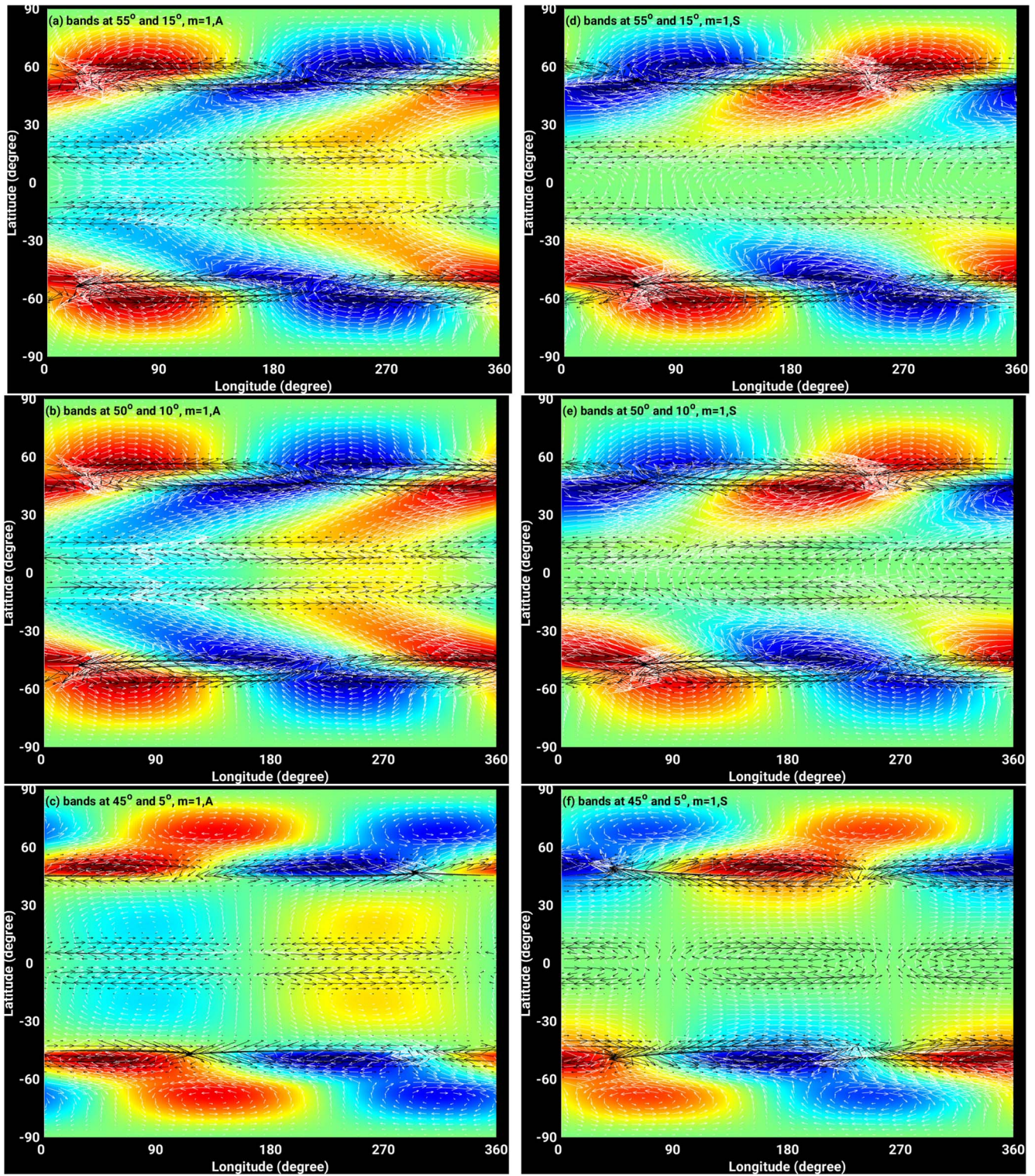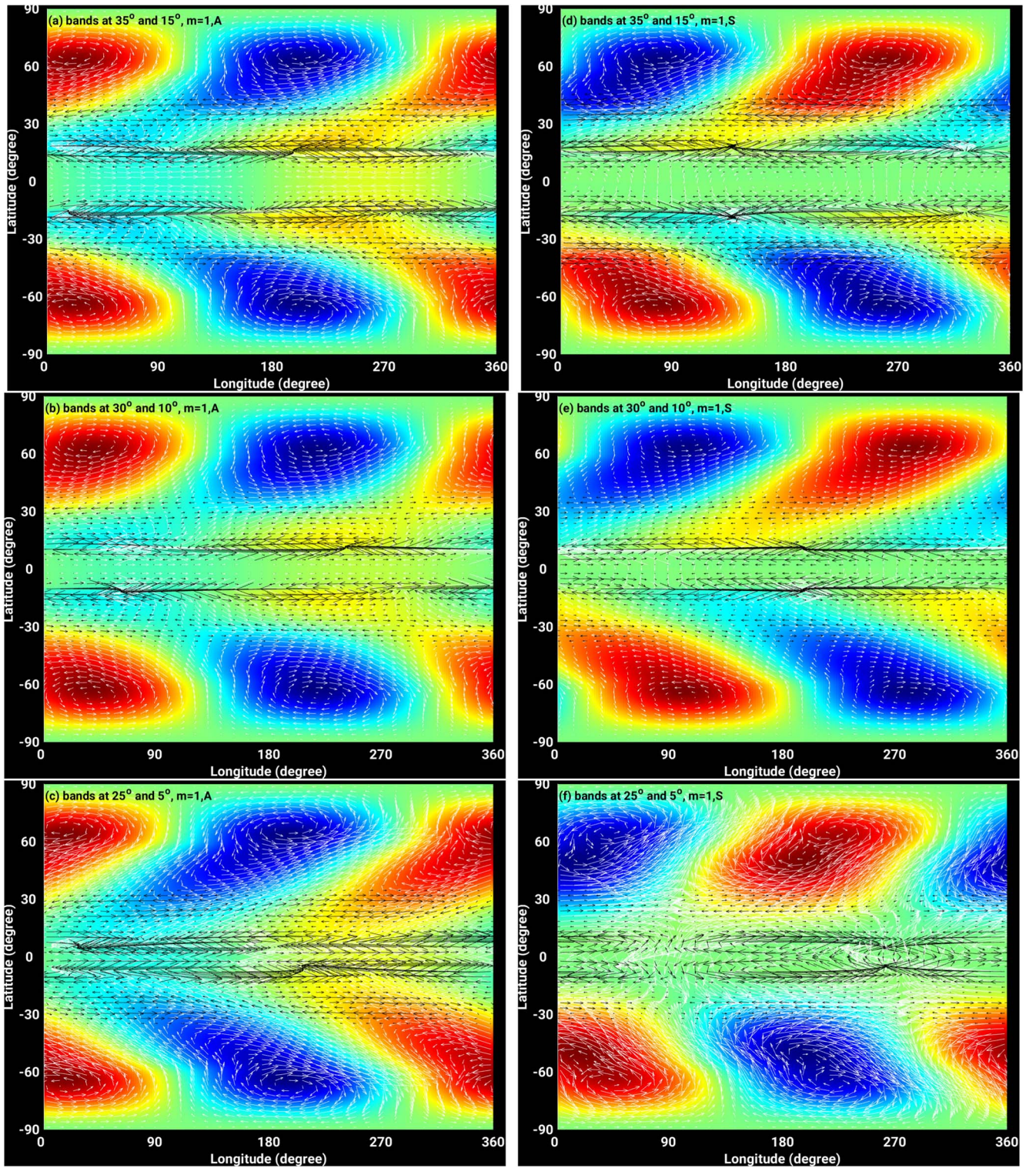
Figure 4. Snapshots of flows (white arrow vectors) and magnetic fields (black arrow vectors) overlaid on top-surface of the shell (color-map) in latitude–longitude planform for the antisymmetric and symmetric $m = 1$ modes, respectively, in left-hand and right-hand columns, for toroidal field bands separated by 40°. For all panels, the high-latitude band's peak is 10 kG and the low-latitude band's peak is 30 kG. Red-yellow denotes bulging of the tachocline top surface, and green-blue the depression. Panels from top to bottom show how the eigenfunctions evolve as the band system migrates equatorward, keeping the same band separation and band amplitude.

perturbation vector that crosses the equator to connect with the other hemisphere. In reality, modes of both symmetries are unstable, so in a combined solution with both symmetries present, there will be both velocity and magnetic connections between the hemispheres. A nonlinear simulation would map

out the details of how this cross-equatorial teleconnection works.

Figure 5 shows a typical progression of the eigenfunctions moving toward the equator that are separated by only 20°. This could represent a situation on the Sun where there were slightly

Figure 5. Snapshots of flows (white arrow vectors) and magnetic fields (black arrow vectors) overlaid on the top-surface of the shell (color-map) in latitude–longitude planform for the antisymmetric and symmetric $m = 1$ modes, respectively, in left-hand and right-hand columns, for toroidal bands separated by 20°. For all panels, the high-latitude band's peak is 10 kG and the low-latitude band's peak is 30 kG. Red-yellow denotes bulging of the tachocline top surface, and green-blue the depressions. Panels from top to bottom display how the eigenfunctions for double-band system always connect between them in each hemisphere, and then eventually allow cross-equatorial communication as the high- and low-latitude bands migrate toward the equator.

overlapping sunspot cycles, or at least a very short minimum between cycles. We see that for both symmetries the interactions between instability of both bands is tightly connected, and by the time the low-latitude band reaches 5° the low-latitude perturbations show very rapid reversals in perturbation velocity and magnetic arrows with latitude, as well as across the equator, while still showing velocity perturbations at higher latitudes that are very broad and tilted with latitude. In this case, the energy is extracted from differential rotation from high-latitudes, where the inflection point is present. The

resulting instability leads to the tilted velocity vectors occurring on the poleward side of the high-latitude band, but still the instability is essentially global, and involves the combination of differential rotation and two toroidal bands in each hemisphere. Here again, without the high-latitude band, the low-latitude band would not be unstable, showing just how important the interaction between bands is in determining how global the MHD instability is, and how different it is from both the single-band and no-band cases. Here, the rise in relative strength of instability of the low-latitude band compared to the higher latitude one, as evidenced by the perturbation arrow lengths, is evident.

3.3. Evolution of Unstable Eigenfunctions Through a Sunspot Cycle

In a real sequence of sunspot cycles, a succession of toroidal field bands would be migrating toward the equator with time and at rates that may be faster in midlatitudes compared to near the equator, while at the same time their peak magnetic fields are changing, rising during the ascending phase and declining during the declining phase. The latitude spacing between the bands probably also changes, becoming narrower in latitude with the equatorward migration. To illustrate how the unstable eigenfunctions might change with time as the sunspot cycle advances, in Figure 6 we show a sequence of three phases, across which the high-latitude band is increasing in peak strength while the low-latitude peak decreases. The band separation drops from $40°$ at the beginning of the sequence to $20°$ at the end of the sequence.

Figure 6 displays dramatic changes in the eigenfunctions of both symmetries of unstable modes from the beginning to the end of the sequence. For symmetric modes, the perturbation velocities and magnetic fields go from being dominant poleward of the low-latitude band to more pronounced in the equatorial domain in both hemispheres at the end of the sequence, when the low-latitude band is at $5°$. For both symmetries, there are strong cross-equatorial interactions, as evidenced by the length of the perturbation arrows. The changes in the antisymmetric modes are even more dramatic because we see that between the first and second planforms in the sequence the most unstable mode switches from longitudinal wavenumber $m = 1$ to $m = 2$. This switching is not unusual; we have seen this before. For example, Table 1 of M. Dikpati et al. (2018b) has presented such a case. This change is coupled with the relative amplitude shifting to much lower latitudes, together with strong perturbation zonal flows in very low latitudes. In the symmetric modes, there are strong cross-equatorial flows.

So, for both symmetries, the connections between the northern and southern hemispheres are particularly strong late in the cycle. In the Sun and in a full nonlinear shallow-water model simulation, several different m modes of both symmetries will be excited, leading to a much more complex picture, including significant differences in the total patterns between north and south. But we expect that the dominant features of individual modes described in Figures 4–6 above would be quite evident in any composite synoptic map, like those for individual modes and individual symmetries about the equator, just more variable and complex.

In some respects, we can think of the toroidal bands as being imposed on Rossby waves in the solar tachocline by the solar dynamo. The band migration toward the equator as a sunspot cycle progresses causes the structure of the unstable MHD Rossby waves to change with time, including which longitudinal wavenumbers are dominant in the wave spectrum. The latitudinal structure of all these unstable waves evolves substantially, with the bands being both a source of instability and forcing their disturbance profiles in latitude to change to accommodate the bands. In turn, this evolving structure, including the bulges and depressions in the top boundary of the shallow-water tachocline model, may determine where in longitude the toroidal fields will most likely emerge from, to manifest as active regions and sunspots at the surface. These emergences are also a part of the dynamo, providing surface magnetic fields that can be advected and diffused to the poles to reverse the sign of the polar fields, providing the seed for the next toroidal band and the next sunspot cycle. Thus, the Rossby waves and dynamo are dynamically linked in some ways, but the dynamo is responsible for the characteristics of the Rossby waves that prevail (see, e.g., a more detailed review on solar Rossby waves and dynamo in Section 5.5 of T. V. Zaqarashvili et al. 2021).

It is well known (see, e.g., M. Dikpati et al. 2007) that although the timing of the peak in a sunspot cycle may differ by up to three years between hemispheres (cycle 24 being a recent example of a three-year difference), the timing of solar minimum is virtually never more than one year apart. This near synchronization between north and south could be caused by the cross-equatorial interactions of MHD Rossby waves, as illustrated in Figures 4–6. Midlatitudes, where maximum solar activity is found, are not so tightly coupled between north and south. Closer to the poles, the generation of a new high-latitude band by the dynamo could vary in timing between hemispheres because it depends on when the polar fields reverse, which in turn is influenced strongly by the amount of magnetic flux carried to the poles from lower latitudes from the previous sunspot cycle.

Since surface meridional circulation is known to vary in amplitude by as much as a factor of two within a sunspot cycle time frame, the rate at which previous active region magnetic flux gets to polar latitudes can vary by a similar amount. We speculate that if the cross-equatorial interaction did not occur in the Sun, it is much more likely that sunspot cycles in the two hemispheres could get substantially out of phase with each other than has been observed over the past several centuries. It is worth recalling that without the second band at high latitudes the low-latitude bands may be stable, limiting the cross-equatorial connection. Thus, the high-latitude bands may help synchronize sunspot cycles in northern and southern hemispheres. If so, then the teleconnections described here are truly global.

### 3.4. Focus on Details of Cross-equatorial Interactions

The cross-equatorial communication between north and south arising from low-latitude MHD Rossby waves is sufficiently important in understanding the Sun's global magnetic structure that in Figure 7 we show synoptic maps constructed by assigning an amplitude to MHD Rossby wave eigensolutions, so that maps can be constructed that show the combination of Rossby waves, differential rotation, and toroidal field. For this purpose, we have chosen the eigenfunctions displayed in Figures 5(c), (f) for toroidal bands positioned at $25°$ and $5°$. We have somewhat arbitrarily assigned a value to the perturbation eigenfunctions, a 10% amplitude relative to
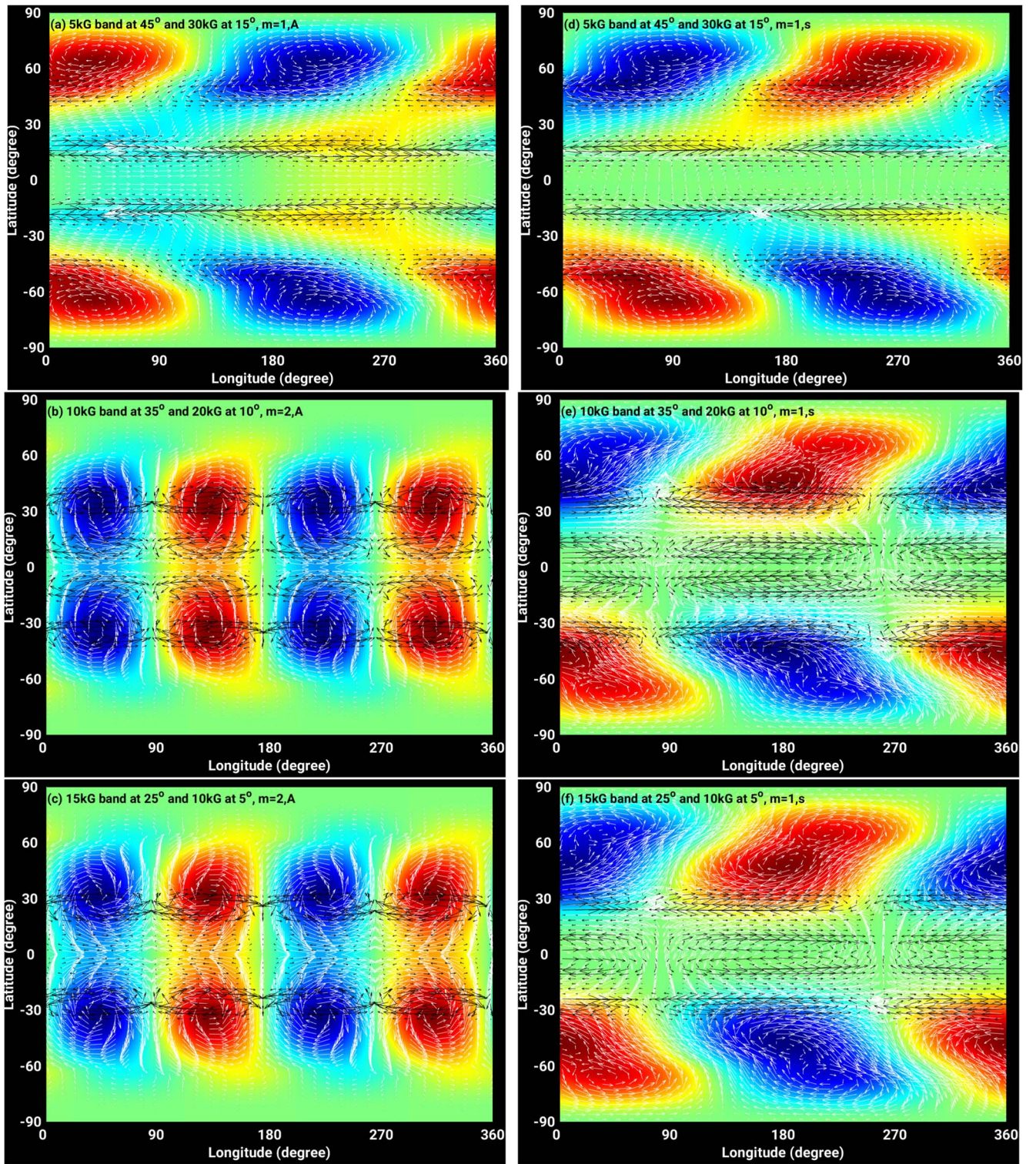
Figure 6. Same as in Figures 4 and 5, but for variable band separation during the band system's equatorward migration; separation between high- and low-latitude bands in each hemisphere decreases from 35° to 20° by the time low-latitude band reaches 5°-latitude. The field-strength of both bands also changes with the frames, as labeled, roughly according to the progress of solar cycle. Note that unstable antisymmetric modes with highest growth rate change wavenumber from $m = 1$ to 2 (bottom two panels in the left-hand column).

the reference state, to illustrate the total velocity and magnetic patterns. Obviously, in a nonlinear simulation this amplitude would be determined internally by the model itself, e.g., in the nonlinear simulations by M. Dikpati et al. (2018b) this amplitude was found to be about 40%. Here, we assigned a modest amplitude of 10%.

Before interpreting Figure 7 in detail, we recall the symmetries about the equator of the velocity and magnetic components for what we have called antisymmetric and symmetric modes. For the antisymmetric mode, the latitude velocity is antisymmetric about the equator, so it has a zero value there. The longitudinal velocity is symmetric about the
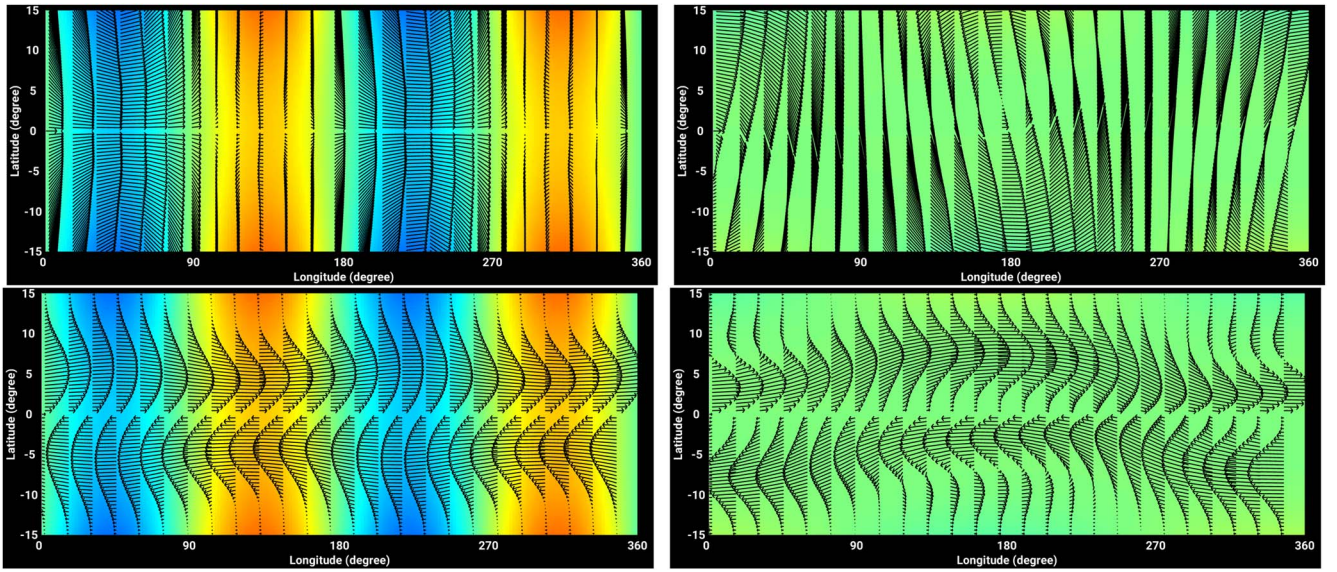
Figure 7. Equatorial region enlarged to display cross-equatorial communication via flows (top panels) and fields (bottom panels) for the case of the bands at 5° and 25° in each hemisphere, i.e., for the cases presented in Figures 5(c) and (f). Again, left-hand and right-hand panels, respectively, display $m = 2$, A and $m = 1$, S. Note that the velocity vectors are also plotted in black arrows instead of white arrows for better visibility. Note that in this enlargement green is the prominent color in the right-hand panels because green implies no bulges or depressions, which is the case near the equator for the symmetric mode. We see this near the equator for all symmetric modes, such as in Figure 5 right-hand panels.

equator. For the antisymmetric modes, the symmetries of the magnetic components about the equator are reversed: the latitudinal field is symmetric, while the longitudinal field reverses sign at the equator. This follows from the antisymmetric reference state toroidal field.

The result of these symmetry properties, seen in Figure 7, is that the total flow (perturbation plus differential rotation) leads for the antisymmetric mode to a pattern of flow to the right of each half wavelength in longitude, alternating with almost no longitudinal flow (Figure 7(a)). By contrast, for the symmetric mode (Figure 7(c)), the perturbation part of the longitudinal flow is adding to differential rotation in one hemisphere while subtracting from it at the same longitude in the opposite hemisphere. The result is a pattern of virtually horizontal velocity arrows extending across the equator at every longitude where the east–west flow is added to differential rotation, resulting in the wavelike pattern seen there. For both symmetries, the latitude velocities are smaller to those in longitude, leading to the nearly horizontal patterns we see. But even though the latitudinal velocities may be small, they still may be important for interactions across the equator. The magnitude of their effects are best determined by nonlinear calculations that are beyond the scope of this paper.

In Figures 7(b), (d) there are analogous patterns for the total magnetic field, with the major difference being that the toroidal fields are much more confined in latitude, consistent with the reference state toroidal bandwidth. In Figure 7(b), we see a sequence of longitudes with total field bulging in latitude, alternating with more constricted total fields, while in Figure 7(d) we get a wavelike pattern again, with an in-phase appearance between the two hemispheres; namely, in one hemisphere the total field is displaced further away from the equator at a longitude, while at the same longitude the total field in the other hemisphere is displaced toward the equator. We see that for modes of both symmetries, there are essentially no magnetic fields crossing the equator. This is a consequence of the linear calculation with the assumption of a purely

antisymmetric toroidal field in the unperturbed state. In a nonlinear calculation, the MHD would be free to push toroidal fields even across the equator or bring oppositely directed toroidal fields together at some longitudes, which is again beyond the scope of this study.

3.5. Properties of Unstable Modes in Relation to Alfvén Wave Speed and Band Separation

In this section, we examine the dependence of the phase speeds and instability intensity (measured by growth rate) of unstable modes on the Alfvén wave speed (which is proportional to peak-field strength) for various band separations. We deliberately fix the low-latitude band at 10° latitude because a single band at this latitude is stable. The presence of a high-latitude band plays the roles of destabilizer of the double-band system. With this choice, we can gain maximum insight about the instability features of a double-band system with high-latitude band placed at various locations.

In Figure 8, we show growth rates and longitudinal phase velocities for cases with the low-latitude band fixed at 10° but varying in peak amplitude from zero to 50 kG, while the high-latitude band is fixed at a strength of 10 kG but placed at 10° intervals from 10° to 60°. Both the 10° and the 60° separations are probably not realistic when compared to observed sunspot cycle patterns, but we include them for completeness. The left-hand column of Figure 8 shows growth rates for all modes, while the right-hand column depicts the phase velocities for the same modes. We have added the phase speed of the local rotation rate, relative to the rotating reference frame, to compare with the disturbance phase speed in the same dimensionless units. At the top of the figure, we have added a dimensional Alfvén wave phase speed that corresponds to the dimensionless peak field at the bottom.

The unstable mode properties depicted in Figure 8 are:

(a) As we have seen in Figures 2 and 3, there are two classes of unstable modes with comparable growth rates, which occur for both equatorial symmetries. One set, from band
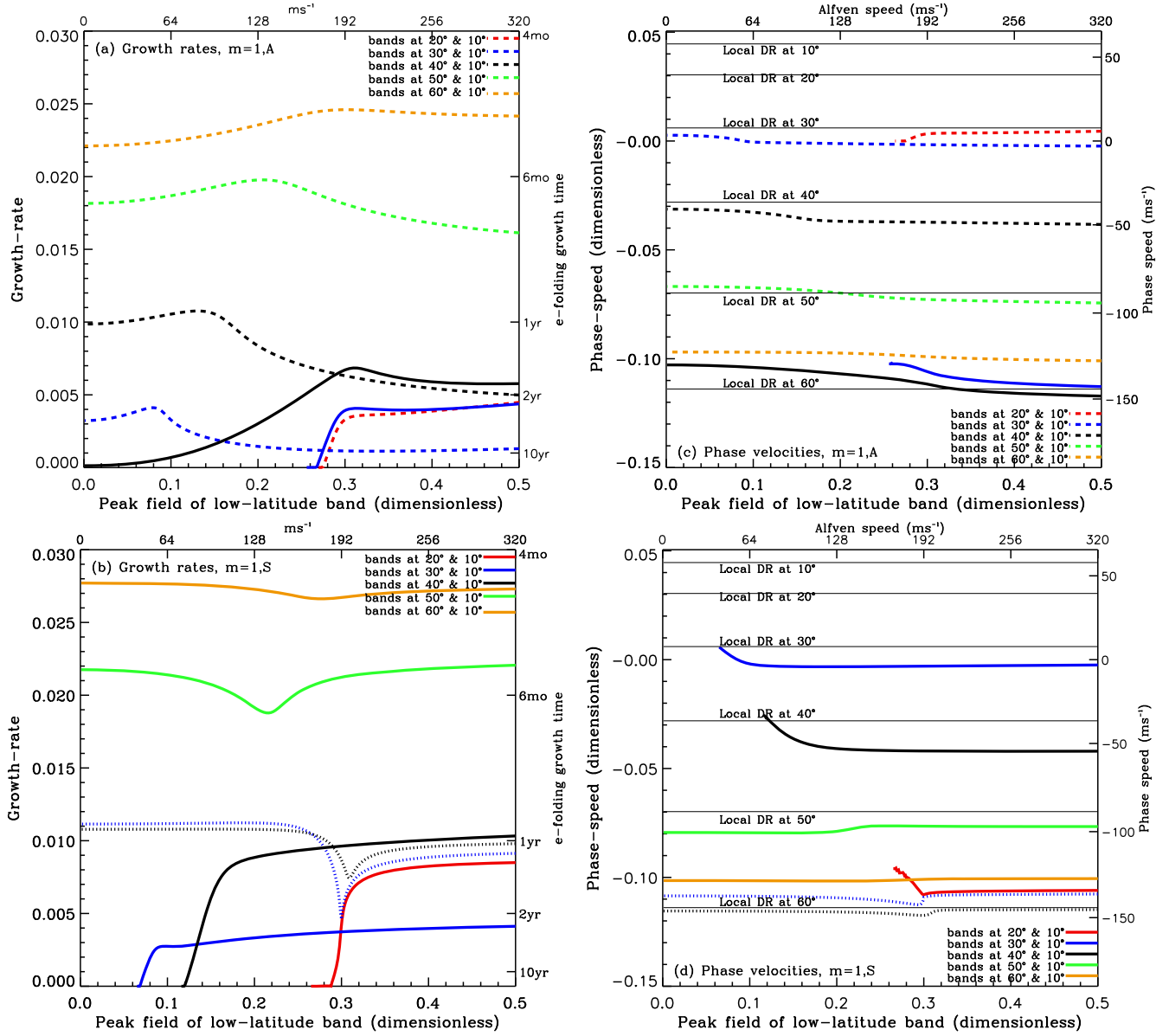
Figure 8. Growth rates (left-hand panels) and phase velocities (right-hand panels) are displayed for a double-band system, for which the low-latitude band (i.e., the active-cycle's band) is placed at 10° and the high-latitude band is placed at five different latitudes, namely at 20°, 30°, 40°, 50°, and 60°. Panels (a) and (c) display growth rates and phase velocities for $m = 1$ antisymmetric modes, and panels (b) and (d) for $m = 1$ symmetric modes. The purpose of keeping the field strength of high-latitude band fixed at 10 kG and varying the strength of low-latitude band is to show how the instability intensity varies with Alfvén speed provided by the low-latitude band's peak-field strength. Furthermore, the choice of placing the low-latitude band at 10° is to demonstrate that the presence of a high-latitude band interacts to make the double-band system unstable when a low-latitude band is not unstable by itself at such a low-latitude. Note that there are two modes with comparable growth rates in two cases, namely when the bands are at 10° and 30°, and are at 10° and 40°. We distinguish these two cases by a dashed–triple–dotted curves as opposed to dashed curves in the antisymmetric case, and by a dotted curves as opposed to solid curves in the symmetric case.

pairs that are relatively close together (10°–30° separations) are present only for low-latitude band's strength above a threshold value. The other set of modes is present for all low-latitude band strengths; it overlaps with the first set, beginning with 20° separation. Both mode types are present, with comparable growth rates, for band separations up to 40°, beyond which only one set of dominant modes is shown for each symmetry. In all cases in which only one unstable mode is present, there may be a second unstable mode, but its growth rate is so low that it is physically insignificant.

(b) The longitudinal phase velocities of the single unstable modes for both symmetries when the bands are separated

by 50° or 60° (green and yellow/orange curves, respectively) are very close to the local rotation rate of the high-latitude band. This indicates that the instability energy source is the magnetic energy of the high-latitude band, together with kinetic energy of the differential rotation profile, which has an inflection point around 60°. Kinetic and magnetic energies can be extracted when there are tilts in velocity vectors and longitudinal phase shifts with latitude between velocity and magnetic vectors. In these cases, the low-latitude toroidal band is also unstable, but it contributes much less energy to the growing modes. Nevertheless, these modes are global, and grow at the same rate everywhere.

(c) High latitude bands placed at 40°, 30°, and 20° lead to two quite different types of unstable modes, which also differ by equatorial symmetry. For unstable antisymmetric modes, the phase velocities are close to the local rotation rate of the higher latitude band location, for all low-latitude band strengths and for band separations of 30° and 20° (dashed black and blue curves). This indicates that the energy for disturbance growth is coming from the high-latitude band. For 20° band separation (blue dashed–triple–dotted curve) the phase speed of the mode is more negative, closely matching the local differential rotation speed near 60°. Here, hydrodynamic instability has taken over, destabilizing both bands. For 10° band separation, phase speed matches the local differential rotation near 30° (see the dashed red curve in panel (c)).

The characteristics of the corresponding equatorially symmetric unstable modes are analogous to their antisymmetric counterparts. The same separation of modes into those present for all low-latitude band peak strengths, and those which require a finite strength of low-latitude band to be unstable, is still present, though some details differ. For band separations of 40° and 50°, modes have the highest growth rates and phase speeds close to the rotation rate of the high-latitude band location. For smaller band-separations, the two unstable modes are distinguishable in a similar way, one type having phase speeds closer to the local rotation rate at higher latitude than both bands, and the other with phase speed close to the rotation at the high-latitude band.

To discuss the global structures of eigenfunction we pick a representative case. Figure 9 shows the eigenfunctions for the two characteristic symmetric modes with comparable growth rates when the bands are at 10° and 40°. The upper panel (a) shows the eigenfunction for the mode with phase speed matching the local rotation rate around 40°, while the lower panel (b) shows the unstable mode with phase speed matching the local rotation speed around 60°. The slower propagating mode (panel (a)) shows no tilts in velocity vectors (white arrows) but significant phase shift between velocity and magnetic vectors, indicating that the energy for this mode comes primarily from the magnetic fields. In this mode, there are essentially no perturbation velocities poleward of about 60°. By contrast, for the eigenfunction in panel (b), we can clearly see the tilted perturbation velocity patterns poleward of the high-latitude band, extending nearly to the pole, showing that angular momentum is being transported to higher latitudes by Reynolds stresses in the wave, thereby extracting kinetic energy out of the differential rotation to drive the instability. Judging by the lengths of the perturbation fields, mostly in longitude, for both modes, more magnetic energy is being extracted from the high-latitude band than from the one at low latitudes—but both are unstable with the same growth rate, however, for growing modes.

Note that the instability intensity (measured by growth rates) increases as the band separation increases (see, for example, the left-hand panels (a) and (b) in Figure 8). This is because the maximum gradient in the differential rotation being at $\sim$60°, more kinetic energy is available for extraction by the perturbation the closer the high-latitude band is to 60°.

Finally, Figure 8 shows that both growth rates and phase speeds depend only very mildly on the Alfvén Speeds. This is because we are analyzing unstable modes. For the neutral modes, the phase speed depends on both classical hydrodynamic Rossby waves' speed (v_{HD}) and Alfvén speed (v_A) following the relation, $v = 1/2(v_{HD} \pm \sqrt{v_{HD}^2 + 4v_A^2})$ (B. Raphaldini et al. 2019; M. Dikpati et al. 2020). Therefore, for zero magnetic field the phase speed matches the classical Rossby waves' phase speed v_{HD}, while for zero rotation the phase speed matches that of pure Alfvén waves v_A. However, for growing modes, the phase speeds are also modified by the differential rotation and are closer to the local rotation rate near the band latitude, therefore the strong dependence on the Alfvén wave speeds is not seen in this case.

4. Summary and Conclusions

There is increasing evidence, reviewed in the introduction, that there are typically two toroidal field bands in each hemisphere—a low-latitude band that is producing spots and a high-latitude band from which other magnetic features are emerging, foretelling of the next sunspot cycle. The combination of spots and other magnetic features in high latitudes is often characterized as the "extended" solar cycle, which has recently been shown to contain predictive capability for the upcoming solar activity cycle's features, namely the strength and timing of the peak of the cycle (S. M. McIntosh et al. 2020). In particular, the authors suggested a linear relationship between the timing of the terminator and the peak-strength of the following cycle. Solar cycle 25 was predicted slightly higher in 2020 (S. M. McIntosh et al. 2020) based on the predicted terminator. However, the prediction was revised (S. W. McIntosh et al. 2023) to be lower than the initial prediction in 2020 after the observation of the terminator of cycle 24, but still higher than that predicted by NOAA/NASA prediction panel, and is more compatible with the current stage of solar cycle 25.

Here, we have used an MHD shallow-water model for the solar tachocline to study the instability of the combination of latitudinal differential rotation and two toroidal bands present in each hemisphere. We have found that having two toroidal bands present leads to complex interactions between low and high-latitude bands in one hemisphere, as well as between low-latitude bands across the equator.

These interactions between the double bands in each hemisphere leads to global unstable modes that are generally quite different from the case when there is a single toroidal band in each hemisphere. The details depend strongly on the amount of latitudinal separation between bands and the relative strength of each band. There are domains for which the high-latitude band governs the instability of the low-latitude band, and vice versa. Results are different for modes with opposite symmetry about the equator, but there are analogous properties too.

The complexity of the instability of the double band system stems from the fact that there are multiple reservoirs of energy in the unperturbed state that are available to drive the instability. Energy from the differential rotation is extracted most readily if the mode phase speed in longitude is close to that of the local differential rotation, namely near 60°. We found that the growth rates and phase speeds of the unstable modes depend strongly on the band location and band separation, but only mildly on the magnetic field strength (Alfvén wave speeds).

As a solar cycle progresses, the spacing between the bands is expected to shrink and the amplitude of both bands will also change. Thus, the progress of bands toward the equator results in constantly evolving dominant modes of instability, including a change in preferred longitudinal wavenumber. Consequently, the degree of connection between low and high latitudes and across the equator also changes. Low-latitude bands that would be stable
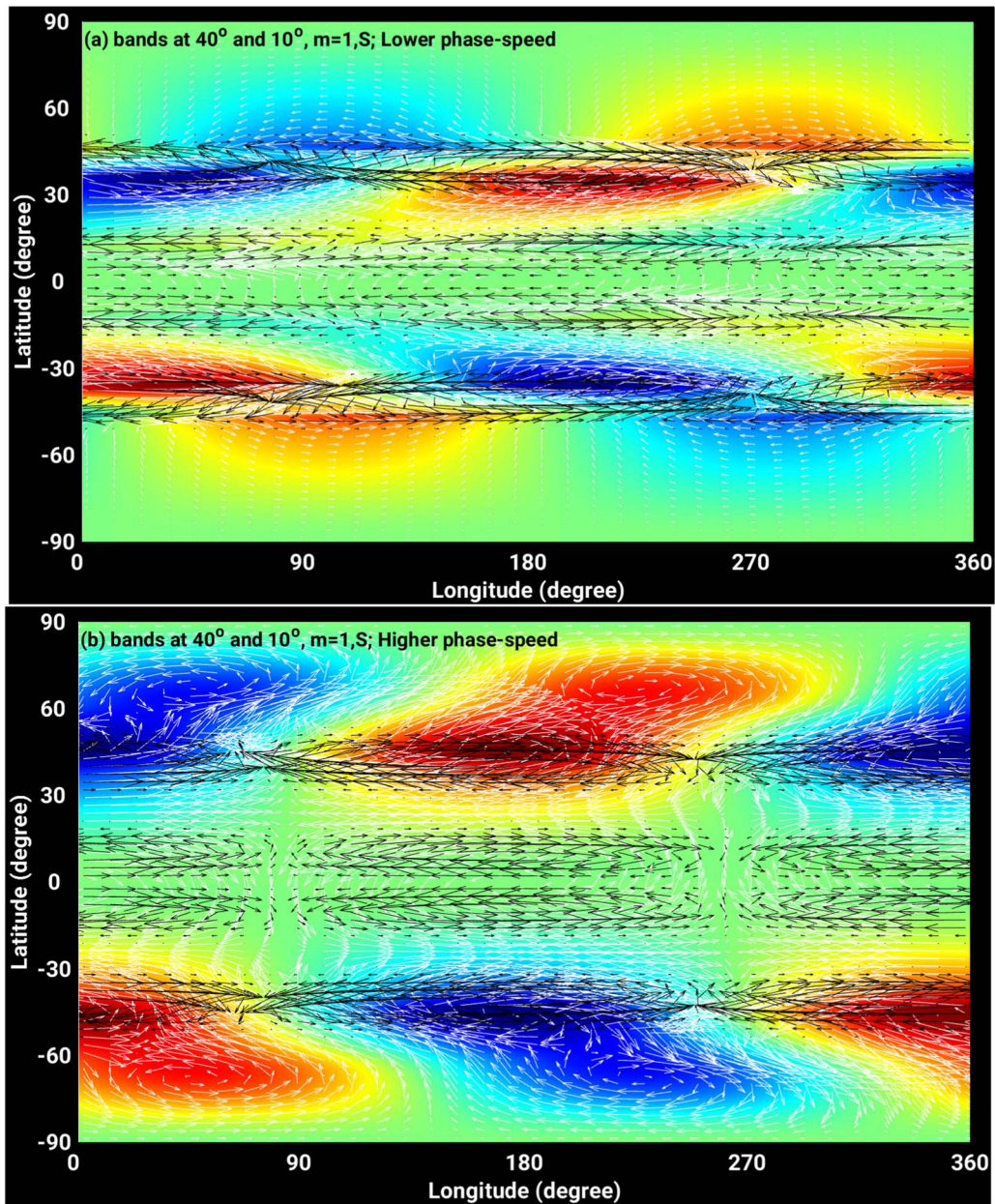
Figure 9. Eigenfunctions displayed in latitude–longitude space for two distinct modes of similar growth rates for the double-band system when a high-latitude band is at 40° and the low-latitude one is at 10° latitudes. The low-latitude band's field-strength is 0.3 in dimensionless unit, or 30 kG dimensional; as in earlier Figures, the high-latitude band's field-strength is 10 kG. Eigenfunctions in top and bottom panels respectively correspond to the cases with solid and dotted black curves in panels (c), (d) of Figure 8. Note that these solid and dotted curves in panel (d) of Figure 8 respectively display lower and higher phase speeds. Latitude–longitude structures look quite different for these two modes.

in the absence of a new high-latitude band are kept unstable by interaction with the new high-latitude band. This can clearly affect the timing of the end of a sunspot cycle. Interactions between unstable bands across the equator can help synchronize solar minimum in the northern and southern hemispheres, which is observed to differ by no more than one year, while sunspot maximum is seen to vary between hemispheres by up to three years. The length of the minimum phase in each hemisphere may also be affected by the timing of formation of the next high-latitude toroidal band in each hemisphere.

The cross-equatorial interactions due to unstable MHD Rossby waves are particularly complex. Depending on mode symmetry about the equator, instability at low latitudes can modify the background toroidal field by warping it away from a flat ring

concentric with the rotation axis, as well as introduce latitudinal bulges and constrictions in it. These changes are accompanied by modifications in the differential rotation that include periodic speeding up and slowing down of the differential rotation for one symmetry, and a periodic oscillation between hemispheres of the maximum zonal flow. In addition, one symmetry provides north–south flow across the equator, while the other has analogous north–south magnetic perturbations. Thus, both kind of symmetries in the unstable modes provide a plausible physical mechanism for magnetic teleconnections in the Sun. In the linear case, these are constrained by the narrowness of the band in each hemisphere. Each of these properties of unstable eigensolutions combined with differential rotation and toroidal bands will acquire finite amplitudes, and evolve further, in a nonlinear simulation. These

effects will further tie the two hemispheres together, as well as connect low and high latitudes with each other in each hemisphere.

Through extensive research, the links between two widely separated regions in the Earth's oceanic systems and also in the atmosphere have been attributed to the teleconnection mechanism, the physical foundation of which relies on the terrestrial Rossby waves. In the Sun, and also between the Sun and the Earth through the interplanetary region, evidence of magnetic teleconnection mechanism has been found (S. W. McIntosh et al. 2021; U. B. I. Ugwu 2022). Physical foundation behind the magnetic teleconnection can be attributed to the magnetically modified Rossby waves. Alternatively, in some cases, though the links among widely separated geographical locations, such as Siberia, Europe, North America, China, and West Africa, were found through the analysis magnetic susceptibility data, the connections may not be via magnetically modified Rossby waves, instead those links were attributed to climatological teleconnection through flows and events (M. E. Evans et al. 2003). We conclude that many properties of global instability of combined differential rotation and multiple toroidal field bands play important roles in producing magnetic teleconnection between the two hemispheres across the equator. This has profound impact on the timing, evolution, and amplitude of solar magnetic cycles.

The present work reveals the role of Rossby waves in promoting cross-equatorial interactions, as well as interactions between different latitudes. Other recent works have suggested similar roles of Rossby waves in the longitudinal organization of photospheric magnetic fields (B. Raphaldini et al. 2023), sunspot groups, as well as recurrent active region emergences at the same location (M. Dikpati & S. W. McIntosh 2020; M. Dikpati et al. 2021; B. Raphaldini et al. 2023) and sympathetic flares, i.e., flares occurring at different regions of the Sun in a short interval (Y. J. Moon et al. 2002; R. Mawad & X. Moussas 2022). This highlights the importance of properly representing and monitoring active Rossby waves (by combining observations and numerical models) in understanding and predicting the magnetic activity of the Sun.

Acknowledgments

ORCID iDs

Mausumi Dikpati https://orcid.org/0000-0002-2227-0488
Bernadett Belucz https://orcid.org/0000-0002-0040-1790
Robertus Erdélyi https://orcid.org/0000-0003-3439-4127
Peter A. Gilman https://orcid.org/0000-0002-1639-6252
Scott W. McIntosh https://orcid.org/0000-0002-7369-1776
Breno Raphaldini https://orcid.org/0000-0002-0744-9746

References

Altrock, R. C. 1988, in Solar and Stellar Coronal Structure and Dynamics, ed. R. C. Altrock (Boulder, CO: National Solar Observatory), 414
Belucz, B., Dikpati, M., McIntosh, S. W., Leamon, R. J., & Erdélyi, R. 2023, ApJ, 945, 32
Bocchino, G. 1933, Oss. Mem. dell'Osservatorio astrofisico Arcetri, 51, 5
Boers, N., Goswami, B., Rheinwalt, A., et al. 2019, Natur, 566, 373
Cally, P. S., Dikpati, M., & Gilman, P. A. 2003, ApJ, 582, 1190
Cliver, E. W. 2014, SSRv, 186, 169
Dikpati, M., Belucz, B., Gilman, P. A., & McIntosh, S. W. 2018a, ApJ, 862, 159
Dikpati, M., & Charbonneau, P. 1999, ApJ, 518, 508
Dikpati, M., & Gilman, P. A. 1999, ApJ, 512, 417
Dikpati, M., & Gilman, P. A. 2001, ApJ, 551, 536
Dikpati, M., Gilman, P. A., Chatterjee, S., McIntosh, S. W., & Zaqarashvili, T. Z. 2020, ApJ, 896, 141
Dikpati, M., Gilman, P. A., de Toma, G., & Ghosh, S. S. 2007, SoPh, 245, 1
Dikpati, M., Gilman, P. A., & Rempel, M. 2003, ApJ, 596, 680
Dikpati, M., & McIntosh, S. W. 2020, SpWea, 18, e2018SW002109
Dikpati, M., McIntosh, S. W., Bothun, G., et al. 2018b, ApJ, 853, 144
Dikpati, M., McIntosh, S. W., Chatterjee, S., et al. 2019, NatSR, 9, 2035
Dikpati, M., McIntosh, S. W., Chatterjee, S., et al. 2021, ApJ, 910, 91
Evans, M. E., Rutter, N. W., Catto, N., Chlachula, J., & Nyvlt, D. 2003, Geo, 31, 537
Gilman, P. A. 2000, ApJL, 544, L79
Gilman, P. A. 2018, ApJ, 853, 65
Gilman, P. A., & Fox, P. A. 1997, ApJ, 484, 439
Guerrero, G. A., Smolarkiewicz, P. K., de Gouveia Dal Pino, E. M., Kosovichev, A. G., & Mansour, N. N. 2016, ApJL, 828, L3
Hansen, R., & Hansen, S. 1975, SoPh, 44, 225
Harvey, K. L., & Martin, S. F. 1973, SoPh, 32, 389
Haurwitz, B. 1940, JMR, 3, 254
Hoskins, B. J., & Ambrizzi, T. 1993, JAtS, 50, 1661
Hoskins, B. J., & Karoly, D. J. 1981, JAtS, 38, 1179
Howard, R., & Labonte, B. J. 1980, ApJL, 239, L33
Kagan, D., & Wheeler, J. C. 2014, ApJ, 787, 21
Klimachkov, D. A., & Petrosyan, A. S. 2017, JETP, 125, 597
Leamon, R. J., McIntosh, S. W., & Marsh, D. R. 2021, E&SS, 8, e2020EA001223
Legrand, J. P., & Simon, P. A. 1981, SoPh, 70, 173
Leroy, J. L., & Noens, J. C. 1983, A&A, 120, L1
Lorenz, E. N. 1951, J. Meteor., 8, 52
Mamatsashvili, G., Stefani, F., Hollerbach, R., & Rudiger, G. 2019, PhRvF, 4, 103905
Martin, S. F. 2018, FrASS, 5, 17
Mawad, R., & Moussas, X. 2022, Ap&SS, 367, 107
McIntosh, S. M., Chapman, S. C., Leamon, R. J., Egeland, R., & Watkins, N. W. 2020, SoPh, 293, 163
McIntosh, S. W., Leamon, R. J., & Egeland, R. 2023, FrASS, 10, 1050523
McIntosh, S. W., Leamon, R. J., Egeland, R., et al. 2021, SoPh, 296, 189
Moon, Y. J., Choe, G. S., Park, Y. D., et al. 2002, ApJ, 574, 434
Raphaldini, B., Dikpati, M., & McIntosh, S. W. 2023, ApJ, 953, 156
Raphaldini, B., Dikpati, M., Norton, A. A., et al. 2023, ApJ, 958, 175
Raphaldini, B., Teruya, A. S., Raupp, C. F. M., & Bustamante, M. D. 2019, ApJ, 887, 1
Snodgrass, H. B., & Wilson, P. R. 1987, Natur, 328, 696
Srivastava, A. K., McIntosh, S. W., Arge, N., et al. 2018, FrASS, 5, 38
Strugarek, A., Belucz, B., Brun, A. S., Dikpati, M., & Guerrero, G. 2023, SSRv, 219, 87
Tappin, S. J., & Altrock, R. C. 2013, SoPh, 282, 249
Teruya, A. S. W., Mayta, V. C., Raphaldini, B., Silva Dias, P. L., & Sapucci, C. R. 2024, Meteorology, 3, 141
Teruya, A. S. W., Raphaldini, B., & Raupp, C. F. M. 2022, FrASS, 9, 856912
Trenberth, K. E., Branstator, G. W., Karoly, D., et al. 1998, JGR, 103, 14291
Ugwu, U. B. I. 2022, European Journal of Applied Physics, 4, 57
Umurhan, O. 2008, A&A, 489, 953
Vasil, G. M., Lecoanet, D., Augustson, K., et al. 2024, Natur, 629, 769
Wallace, J. M., & Gutzler, D. S. 1981, MWRv, 109, 784
Weber, M. A., Fan, Y., & Miesch, M. S. 2013, SoPh, 287, 239
Wilson, P. R. 1987, SoPh, 110, 1
Zaqarashvili, T. V., Albekioni, M., Ballester, J. L., et al. 2021, SSRv, 217, 15
Zaqarashvili, T. V., Oliver, R., Ballester, J. L., & Shergasvili, B. M. 2007, A&A, 470, 815